PHYSICAL REVIEW B **96**, 094522 (2017)

Pair breaking of multigap superconductivity under parallel magnetic fields in the electric-field-induced surface metallic state

Masahiro Nabeta,[1] Kenta K. Tanaka,[1] Seiichiro Onari,[1,2] and Masanori Ichioka[1,2]
[1]*Department of Physics, Okayama University, Okayama 700-8530, Japan*
[2]*Research Institute for Interdisciplinary Science, Okayama University, Okayama 700-8530, Japan*
(Received 6 March 2017; revised manuscript received 28 July 2017; published 19 September 2017)

The roles of paramagnetic and diamagnetic pair-breaking effects in superconductivity in the electric-field-induced surface metallic state are studied using the Bogoliubov–de Gennes equation when magnetic fields are applied parallel to the surface. The multigap states of the subbands are related to the depth dependence and the magnetic field dependence of the superconductivity. In the Fermi-energy density of states and the spin density, subband contributions successively appear from higher-level subbands with increasing magnetic fields. The characteristic magnetic field dependence may be a key feature to identify the multigap structure of the surface superconductivity.

DOI: 10.1103/PhysRevB.96.094522

I. INTRODUCTION

Electric-field-induced carrier doping by the field-effect-transistor structure or the electric-double-layer-transistor (EDLT) structure [1–6] is a new powerful method to control the carrier density with the gate voltage. At surfaces of insulators or semiconductors, carriers are induced near the surface by the strong electric field and trapped in the confinement potential of the electric field. In the surface metallic states by the EDLT, superconductivity is realized at low temperatures [1], as performed in $SrTiO_3$ [2], ZrNCl [3], $KTaO_3$ [4], and MoS_2 [5,6]. The surface superconductivity in $SrTiO_3$ was also realized at the interface of $LaTiO_3/SrTiO_3$ and $LaAlO_3/SrTiO_3$ [7,8].

The unique nature of the surface metallic state is that subbands are formed by the quantum confinement of carriers near the surface [2,9,10]. This is different in nature from three-dimensional bulk metals or ideal two-dimensional systems. The surface superconductivity is expected to have multigaps depending on the subbands [11]. The subband-dependent multigaps are tightly related to the spatial variation of the superconductivity along the depth direction. It is also suggested that crossover from the BCS pair to the Bose-Einstein condensate (BEC) occurs in one of the subbands [11]. The multigap and the BCS-BEC crossover are universal features in superconductivity within nanoscale quantum confinement [12,13]. In many previous studies, superconductivity in nanoscale quantum confinement was considered in the potential well $V(\mathbf{r}) = 0$ inside of the confinement and $V(\mathbf{r}) \to \infty$ at the boundary [12–16]. However, in the surface superconductivity in the EDLT structure we have to consider the spatial variation of $V(\mathbf{r})$ such as in the triangular potential. There wave functions of the electronic states were studied in the electric-field-induced surface metallic states [2,9,10]. The superconductivity in this case is studied with a method using the Bogoliubov–de Gennes (BdG) equation, as in Refs. [11,17]. This method was also used in theoretical studies [18,19] to explain the spatial structure of the superfluidity of a fermionic atomic gas trapped in a harmonic potential [20,21].

On the other hand, measurements of physical properties related to the pair breaking by magnetic fields are important methods to understand the character of each superconducting system. The surface superconductivity in the EDLT structure was identified as a two-dimensional one from the magnetic field orientation dependence of the upper critical field [22]. This indicates that vortices do not penetrate into the narrow surface superconducting region when a magnetic field is applied parallel to the surface.

The purpose of this paper is to study the pair breaking of the surface superconductivity when magnetic field is applied parallel to the surface and to clarify how influences of the subband-dependent multigap superconductivity appear in the magnetic field H. We calculate properties of the surface superconductivity using the BdG equation [11,17], assuming isotropic s-wave pairing. In addition to the paramagnetic pair breaking by the Zeeman shift of the Fermi energy level between up and down spins, we study the effects of the diamagnetic pair breaking from the screening current induced by applied magnetic fields. In Ref. [23], only the paramagnetic pair-breaking effect was studied in the case of the confinement potential including the screening effect of electric fields by carriers. Since the diamagnetic pair-breaking effect was not considered in previous studies, it is necessary to clarify the contributions of diamagnetic effects as another mechanism of pair breaking under parallel magnetic fields.

This paper is organized as follows. We explain our theoretical formulation of the BdG equation under parallel magnetic fields in Sec. II and the Appendix. We study the influence of magnetic fields on the pair potential in Sec. III. Section IV discusses current, spin current, and internal field. As phenomena reflecting the multigap superconductivity of the subband system, the magnetic field dependence of electronic states and paramagnetic spin density in the surface superconductivity are discussed in Secs. V and VI, respectively. The last section is devoted to the summary.

II. BOGOLIUBOV–DE GENNES EQUATION UNDER PARALLEL MAGNETIC FIELDS

In this paper, we calculate the pair potential $\Delta(\mathbf{r})$ and the wave functions $u_\epsilon(\mathbf{r})$, $v_\epsilon(\mathbf{r})$ for the eigenenergy E_ϵ using the BdG equation [17]. Notes on the derivation of the BdG equation and the related equations in the presence of the

paramagnetic effect are given in the Appendix. In our coordinates $\mathbf{r} = (x,y,z)$, the z axis is the depth direction perpendicular to the surface at $z = 0$. For the confinement potential near the surface, we use the triangular potential, $V(z) = |e|F_0 z$ for $z > 0$ and $V(z) \to \infty$ for $z \leqslant 0$. We typically consider the case of sheet carrier density $n_{2D} = 6.5 \times 10^{13}$ cm^{-2}, electric field $F_0 = 1.4 \times 10^{-3}$ V/nm at the surface, and a single band with effective mass $m^* = 4.8m_0$, where m_0 is the free electron's mass. This corresponds to one of the cases studied in Ref. [11] considering $SrTiO_3$.

We set the vector potential as $\mathbf{A} = (0,A_y,0)$, with $A_y = -Hz$, so that the magnetic field parallel to the surface is applied along the x direction, and the screening current flows along the y direction. In this situation, we can set $\Delta(\mathbf{r}) = \Delta(z)e^{i2qy}$ and

$$\begin{pmatrix} u_\epsilon(\mathbf{r}) \\ v_\epsilon(\mathbf{r}) \end{pmatrix} = \frac{1}{\sqrt{S}} e^{i(k_x x + k_y y)} \begin{pmatrix} u_\epsilon(z)e^{iqy} \\ v_\epsilon(z)e^{-iqy} \end{pmatrix}, \tag{1}$$

where S is a unit of the area of the surface and q is a constant related to the current flow, where we assume that physical quantities do not have y dependence. We do not consider the penetration of vortices. We decide the q value from the current conservation, as explained later in this section. Thus the BdG equation is reduced to

$$\begin{pmatrix} K_+ & \Delta(z) \\ \Delta(z) & -K_- \end{pmatrix} \begin{pmatrix} u_\epsilon(z) \\ v_\epsilon(z) \end{pmatrix} = E_\epsilon \begin{pmatrix} u_\epsilon(z) \\ v_\epsilon(z) \end{pmatrix}, \tag{2}$$

with the kinetic term

$$K_\pm = \frac{\hbar^2}{2m^*}\left[k_x^2 + \left(\pm k_y + q + \frac{\pi}{\phi_0}A_y\right)^2 - \partial_z^2\right] + V(z) \mp \mu_B H - \mu, \tag{3}$$

where ϕ_0 is a flux quantum and $\pm\mu_B H$ is the Zeeman energy with the Bohr magneton $\mu_B = 5.7883 \times 10^{-5}$ eV/T. The chemical potential μ ($\sim E_F$, the Fermi energy) is determined to fix n_{2D}. The eigenstates of Eq. (2) are labeled by $\epsilon \equiv (k_x,k_y,i_z,\alpha)$, where i_z ($= 1,2,\dots$) indicates the label for subbands coming from quantization by confinement in the z direction and α is for two states of particle and hole branches. For the boundary condition at the surface, we set $u_\epsilon(z) = v_\epsilon(z) = 0$. In the following, energy, length, magnetic field, and local carrier densities are, respectively, presented in units of meV, nm, T, and nm^{-3}.

The pair potential is calculated by the gap equation

$$\Delta(z) = V_{\rm pair}{\sum_\epsilon}' u_\epsilon(z)v_\epsilon(z)f(-E_\epsilon) \tag{4}$$

with the Fermi distribution function $f(E)$. In Eq. (4), the energy cutoff $E_{\rm cut}$ of the pairing interaction is considered in the summation as $\sum_\epsilon' = \sum_\epsilon \theta(E_{\rm cut} - |E_\epsilon|)$ using the step function θ. Here, we consider a conventional case of spin-independent isotropic s-wave pairing. We typically use $V_{\rm pair} = 0.08$ and $E_{\rm cut} = 10$ meV. These values give the transition temperature $T_c \sim 6.3$ K. We consider this larger-T_c case to ensure energy resolution within the superconducting gap in our calculations. Therefore, gap amplitude and critical field are about 15 times larger than those in the superconductivity of $SrTiO_3$ [2,22], but qualitative behaviors are not significantly changed. While the coherence length is expected to become $\sqrt{15}$ times shorter, the z dependence of $\Delta(z)$ is determined by the spatial variation of the wave functions in the confinement potential, rather than the coherence length, as shown later. The thickness of the surface superconducting region is still narrow, so we neglect the penetration of vortices with the core radius in the order of the coherence length.

The local carrier density $n(z) = n_\uparrow(z) + n_\downarrow(z)$, spin density $m(z) = n_\uparrow(z) - n_\downarrow(z)$, current density $J(z) = J_\uparrow(z) + J_\downarrow(z)$, and spin current density $J_s(z) = J_\uparrow(z) - J_\downarrow(z)$ are calculated from up- and down-spin contributions:

$$n_\uparrow(z) = \sum_\epsilon |u_\epsilon(z)|^2 f(E_\epsilon), \tag{5}$$

$$n_\downarrow(z) = \sum_\epsilon |v_\epsilon(z)|^2 f(-E_\epsilon), \tag{6}$$

$$J_\uparrow(z) = \frac{e\hbar}{m^*}\sum_\epsilon \left(k_y + q + \frac{\pi}{\phi_0}A_y\right)|u_\epsilon(z)|^2 f(E_\epsilon), \tag{7}$$

$$J_\downarrow(z) = \frac{e\hbar}{m^*}\sum_\epsilon \left(-k_y + q + \frac{\pi}{\phi_0}A_y\right)|v_\epsilon(z)|^2 f(-E_\epsilon). \tag{8}$$

Derivations of Eqs. (4)–(8) are explained in the Appendix.

The density of states (DOS) with spin decomposition is obtained as

$$N(E) = N_\uparrow(E) + N_\downarrow(E) = \int_0^\infty N(E,z)dz \tag{9}$$

from the local DOS $N(E,z) = N_\uparrow(E,z) + N_\downarrow(E,z)$ by

$$N_\uparrow(E,z) = \sum_\epsilon |u_\epsilon(z)|^2 \delta(E - E_\epsilon), \tag{10}$$

$$N_\downarrow(E,z) = \sum_\epsilon |v_\epsilon(z)|^2 \delta(E + E_\epsilon). \tag{11}$$

To identify the roles of paramagnetic and diamagnetic pair-breaking effects, calculations are performed for two cases.

(i) Only the paramagnetic pair-breaking is considered by setting $A_y = q = 0$.

(ii) Both diamagnetic and paramagnetic pair breakings are considered. We set $A_y = -Hz$. From Eqs. (7) and (8), the total current $J_{\rm total} \equiv \int_0^\infty J(z)dz$ is an increasing function of q. We decide the q value so that it satisfies the current conservation $J_{\rm total} = 0$.

In our numerical calculations, we discretize the region $0 < z < 30$ to $N_z = 151$ points, and ∂_z is estimated by differences between neighboring points. Thus we calculate eigenstates of the $2N_z \times 2N_z$ matrix in Eq. (2) under given (k_x,k_y). Since components of the matrix in Eq. (2) are real, wave functions $u_\epsilon(z)$ and $v_\epsilon(z)$ are real functions. Iterating calculations of Eqs. (2) and (4) from an initial state with constant $\Delta(z) = 1.0$ [case (i)] or 0.82 [case (ii)], we obtain self-consistent results of $\Delta(z)$ and wave functions. We study the H dependence of the superconducting state at the low temperature $T = 1.16 \times 10^{-2}$ K $\ll T_c$.

III. PAIR POTENTIAL

First, we study the influence of H on $\Delta(z)$. In Fig. 1(a) we plot the average $\langle\Delta\rangle \equiv \int_0^\infty \Delta(z)n(z)dz / \int_0^\infty n(z)dz$ as a function of H. At lower fields, $\langle\Delta\rangle$ is almost constant. In case (i) with only the paramagnetic effect, $\langle\Delta\rangle$ shows

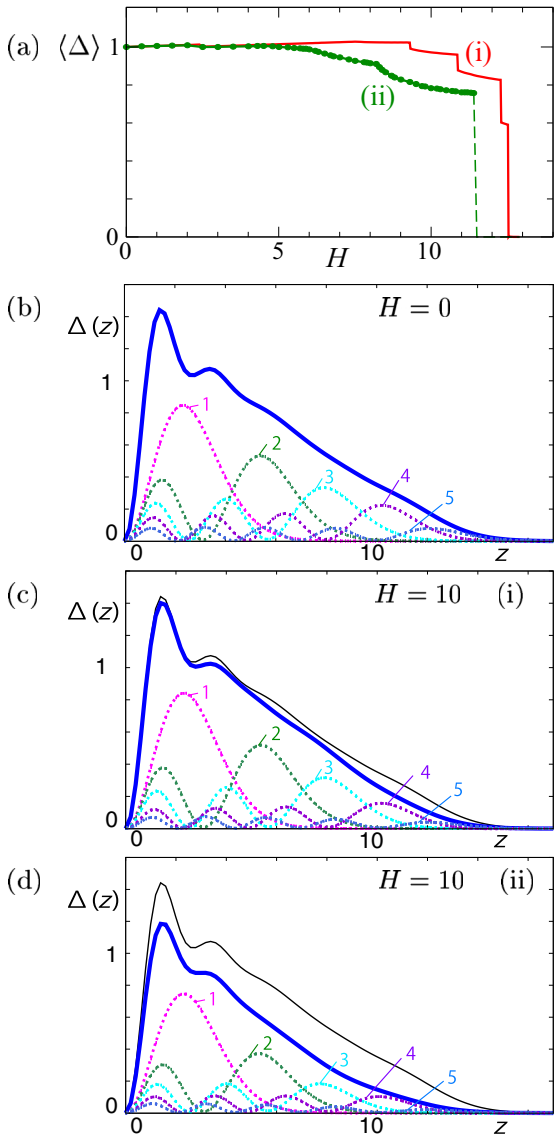

FIG. 1. (a) H dependence of the average $\langle\Delta\rangle$ in cases (i) and (ii). Dashed line for (ii) indicates a possible first-order transition of H_c. (b) Depth z dependence of the pair potential $\Delta(z)$ (thick solid line) and the subband decompositions (dashed lines) to $i_z = 1, \ldots, 5$. $H = 0$. (c) The same as (b), but $H = 10$ in case (i) for only the paramagnetic pair-breaking effect. (d) The same as (b), but $H = 10$ in case (ii) for both paramagnetic and diamagnetic pair-breaking effects. In (c) and (d), thin solid lines are for $H = 0$ for comparison.

steplike suppression at $H > 9$. It suddenly vanishes at the first-order transition of the critical field $H_c \sim 12.5$. This behavior is similar to those suggested for superconductivity within nanoscale quantum confinement [14–16]. In our calculation, the possibility of Fulde-Ferrell-Larkin-Ovchinnikov [24,25] states is not considered. In case (ii), the steplike change is smeared, and further suppression occurs by the additional diamagnetic pair breaking effect at $H > 5$. This indicates that the diamagnetic pair-breaking effect could be another important mechanism for suppression of superconductivity even under parallel magnetic fields. In Fig. 1(a), we use a dashed line to indicate the possible first-order transition of H_c in case (ii) since $\Delta(z) \to 0$ at $H \geqslant 11.5$ in the calculation starting from an initial state with small Δ.

The depth dependences of $\Delta(z)$ and the subband decomposition are presented in Figs. 1(b)–1(d). Reflecting the confinement in $V(z)$, $\Delta(z)$ has a peak at $z \sim 1.2$ and decreases towards zero at $z \sim 15$. With increasing subband index i_z, amplitudes of contributions to $\Delta(z)$ become smaller but extend to a deeper z region. Compared with the case of a zero field in Fig. 1(b), $\Delta(z)$ is weakened at deeper positions for $H = 10$ in Fig. 1(c) because suppression of superconductivity occurs only in higher-level subbands $i_z = 4$ and 5, whose contributions extend to the deeper region. In case (ii) in Fig. 1(d), since the suppression occurs at subbands $i_z = 2, \ldots, 5$, $\Delta(z)$ shows suppression in the whole z region. Therefore subband contributions are related to the depth dependence of the superconducting state.

IV. CURRENT AND SPIN CURRENT

In case (ii), which includes the diamagnetic pair-breaking effect, screening current flows along the y direction parallel to the surface. In this section, we study the current, spin current, internal field, and diamagnetic magnetization. Figure 2(a) shows the depth dependence of spin-dependent currents $J_\uparrow(z)$ and $J_\downarrow(z)$ at $H = 6$. We see small deviations between $J_\uparrow(z)$ and $J_\downarrow(z)$. At the high field $H = 10$ near H_c, the difference between $J_\uparrow(z)$ and $J_\downarrow(z)$ becomes larger, as shown in Fig. 2(b). The depth dependence of the total current $J(z) = J_\uparrow(z) + J_\downarrow(z)$ is presented in Fig. 2(c) at $H = 6$ and 10. The current $J(z)$ flows in order to screen penetration of magnetic fields from outside of the thin superconducting region. Therefore the sign of $J(z)$ changes from the surface region to the deeper z region. The amplitude of $J(z)$ becomes weaker at the high field $H = 10$, as the superconducting pair potential is suppressed by the parallel magnetic field. Spin current $J_s(z) = J_\uparrow(z) - J_\downarrow(z)$ appears in the presence of both paramagnetic and diamagnetic pair-breaking effects. The depth dependence of the spin current $J_s(z)$ is presented in Fig. 2(d) at $H = 6$ and 10. The amplitude of $J_s(z)$ becomes larger with increasing H. An imbalance of up and down spins occurs where superconductivity is partially suppressed. Therefore, the oscillating behavior of $J_s(z)$ at $H = 6$ reflects the oscillation of the wave function in the higher-level subband.

From the total current $J(z)$ in Fig. 2(c), we calculate the variation of internal field as $\delta M(z) = -\int_0^z J(z')dz'$. The depth dependence of $\delta M(z)$ is presented in Fig. 3(a), where the internal field is slightly suppressed inside the superconducting region. At the high field $H = 10$, the width of the superconducting region becomes smaller than that at $H = 6$. Using the definition $z_0 \equiv q\phi_0/\pi H$, we can write $q + \frac{\pi}{\phi_0}A_y = -\frac{\pi}{\phi_0}H(z - z_0)$. For q determined by the condition $J_{\rm total} = 0$, we plot z_0 as a function of H in Fig. 3(b). Since z_0 is located near the center of the superconducting region, z_0 becomes smaller at higher H.

The H dependence of the diamagnetic magnetization $M = \int_0^\infty \delta M(z)dz$ is shown in Fig. 3(c), where M decreases linearly at low fields. It increases towards zero at high fields, reflecting suppression of the pair potential by parallel magnetic fields. We note that M is a tiny quantity since the superconducting

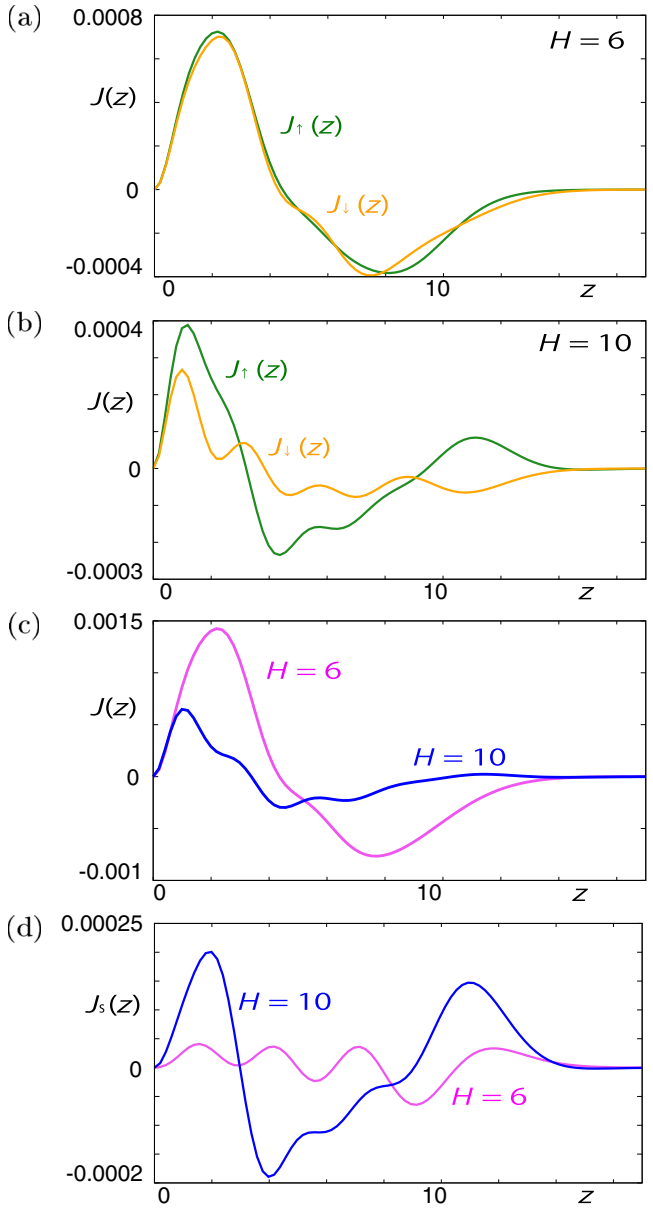

FIG. 2. Depth z dependence of the current. (a) Spin-dependent currents $J_\uparrow(z)$ and $J_\downarrow(z)$ at $H = 6$. (b) $J_\uparrow(z)$ and $J_\downarrow(z)$ at $H = 10$. (c) Total current $J(z)$ at $H = 6$ and 10. (d) Spin current $J_s(z)$ at $H = 6$ and 10. The vertical axis is in units of $e\hbar/m^*$.

region is narrow compared to the penetration length in the surface superconductivity.

V. MAGNETIC FIELD DEPENDENCE OF ELECTRONIC STATES

Because they are phenomena where contributions of multigap superconductivity in the subband system clearly appear, we study the influence of magnetic fields on the electronic states. In Fig. 4(a), we show eigenenergies E_ϵ as a function of $E_\parallel = \hbar^2(k_x^2 + k_y^2)/2m^*$ in case (i). For each subband $i_z = 1,2,\ldots$, there exist two states of particle and hole branches. Line segments with positive (negative) slope are particle (hole) branches with $\int_0^\infty [|u_\epsilon(z)|^2 - |v_\epsilon(z)|^2]dz > 0$

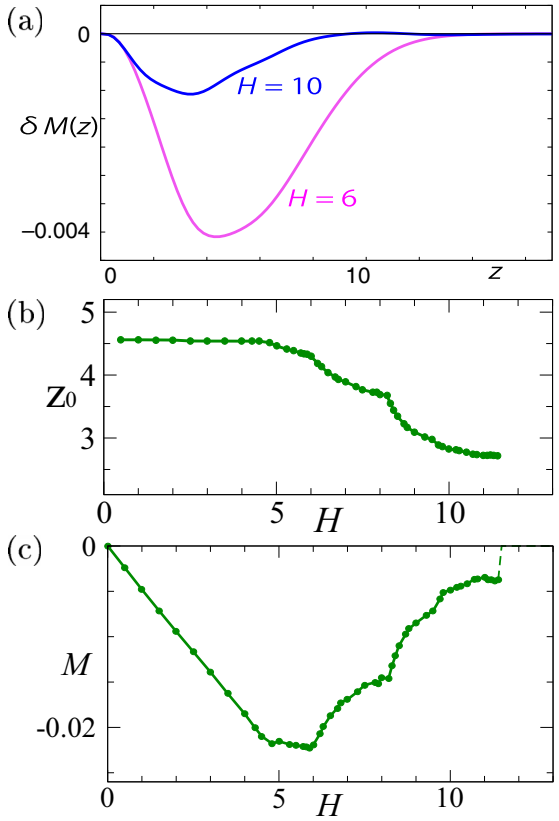

FIG. 3. (a) Variation of internal field. Depth z dependence of $\delta M(z)$ is presented at $H = 6$ and 10. (b) H dependence of $z_0 \equiv q\phi_0/\pi H$ to satisfy the current conservation. (c) H dependence of magnetization M. The vertical axis is in units of $e\hbar/m^*$.

(< 0), where the main contributions come from the up-spin electron's K_+ (the down-spin hole's $-K_-$). At the energy where particle and hole branches cross each other in the normal state as $K_+ = -K_-$, a superconducting gap opens at each subband. The gap amplitude becomes smaller in the higher-level subband, indicating multigap superconductivity [11]. The superconductivity in subband $i_z = 5$ is BEC-like [11–13] since the gap is located at the bottom of the dispersion curve. The center energy of the gap moves from $E = 0$ because of the Zeeman energy. Small gaps also appear at the crossing points of electron and hole branches between different subbands at higher $|E|$.

In Fig. 4(b), hole branches of down-spin electrons are converted to the particle branch as $E_\epsilon \to -E_\epsilon$. Figure 4(b) clearly shows the contribution of the Zeeman shift, i.e., the branches for up (down) spin shift to lower (higher) energy. In Fig. 4(b) at the high field $H = 10$, the Fermi energy E_F is within the superconducting gap of lower-level subbands $i_z = 1$ and 2. However, E_F is outside of the gap edge in the higher-level subband $i_z = 4$ because the small gap in the subband is smaller than the Zeeman shift energy. When the Zeeman shift energy becomes the same order as the largest gap of the lowest subband $i_z = 1$, the superconductivity vanishes at H_c.

These behaviors of the Zeeman shift are reflected also in the DOS $N(E)$ in Fig. 5(a), where finite DOS appears at E_F by

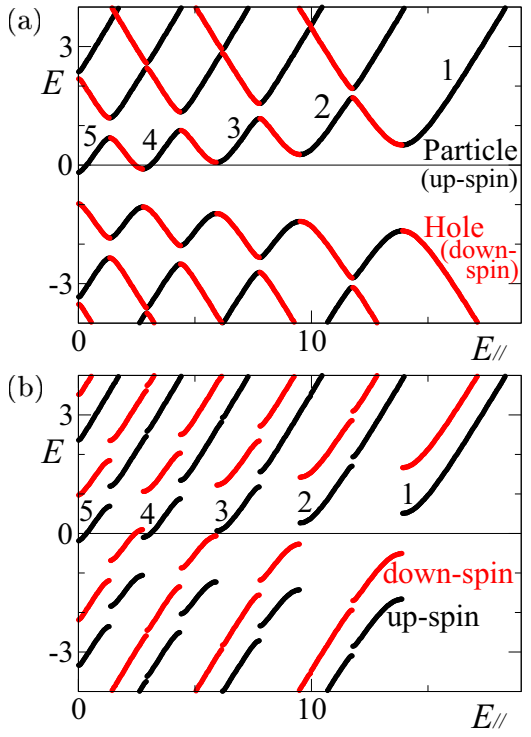

FIG. 4. (a) Eigenenergy E_ϵ as a function of $E_\parallel$ for particle (up-spin) and hole (down-spin) branches of subbands $i_z = 1,2,\ldots$ at $H = 10$ in case (i). Fermi energy E_F corresponds to $E = 0$. (b) Hole branches of down spin are converted to particle branches in order to show dispersion of up- and down-spin electrons for subbands i_z.

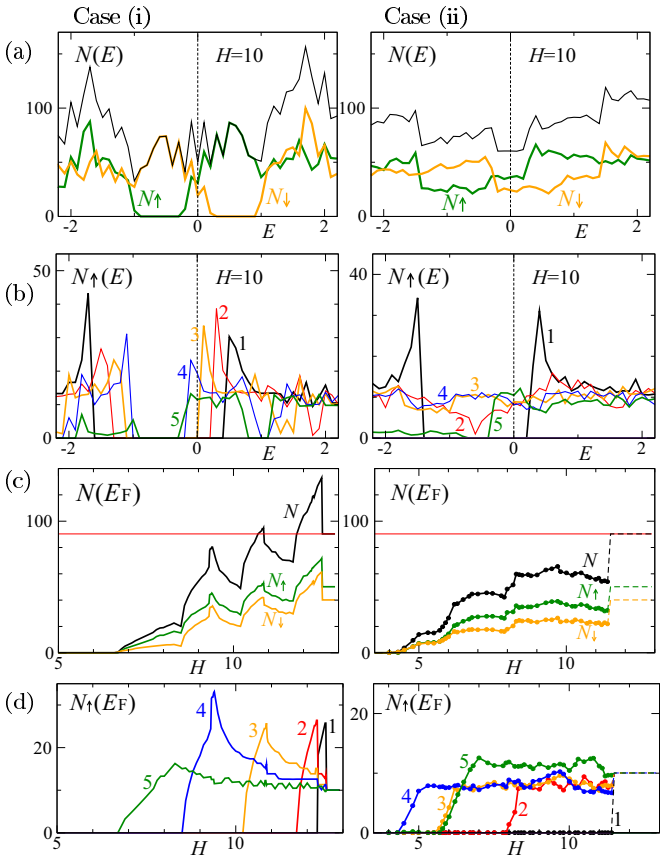

FIG. 5. Electronic state at $H = 10$. Left and right columns are, respectively, for cases (i) and (ii). (a) DOS $N(E)$ with the spin-resolved DOS $N_\uparrow(E)$ and $N_\downarrow(E)$. (b) Subband decompositions ($i_z = 1,\ldots,5$) of $N_\uparrow(E)$. (c) H dependence of Fermi-energy DOS $N(E_F)$ with the spin decompositions $N_\uparrow(E_F)$ and $N_\downarrow(E_F)$. $N(E_F)$ in the normal state is presented by a straight line. (d) Subband decompositions of $N_\uparrow(E_F)$ in (c).

the Zeeman shift of $N_\uparrow(E)$ and $N_\downarrow(E)$. We show the subband decompositions in Fig. 5(b). In case (i), each subband has a finite gap with a sharp peak at the gap edge. Higher-level subbands have a smaller gap, and the gap edges touch E_F by the Zeeman shift. Therefore the Fermi-energy DOS $N(E_F)$ comes from higher-level subbands. On the other hand, in case (ii), the gap is smeared due to the diamagnetic pair-breaking effect, and sharp peaks at the gap edge vanish, except for $i_z = 1$. Thus $N_\uparrow(E)$ and $N_\downarrow(E)$ are gapless in Fig. 5(a).

In Fig. 5(c), we plot $N(E_F)$ with $N_\uparrow(E_F)$ and $N_\downarrow(E_F)$ as a function of H. Subband decompositions of $N_\uparrow(E_F)$ are presented in Fig. 5(d). We note that the contribution of lowest subband $i_z = 1$ does not appear until near H_c. In case (i) in Fig. 5(c), $N(E_F)$ appears at $H > 6$ and increases with multiple-sharp-peak behavior as a function of H. These peaks in the case of triangular confinement potential are contrasted with the behavior in the case in Ref. [23]. The peak in Fig. 5(c) occurs when Zeeman energy $\mu_B H$ equals the gap amplitude of a subband, and E_F touches the sharp peak at the gap edge in Fig. 5(b). Therefore, with increasing H, new contributions of lower-level subbands appear near the peak fields, as seen by the subband decomposition in Fig. 5(d). The multiple-peak behavior of $N(E_F)$ in Fig. 5(c) is also a reason for the step of $\langle\Delta\rangle$ in the H dependence in Fig. 1(a) for case (i). For case (ii) in Fig. 5(c), peak behavior is smeared in the H dependence of $N(E_F)$ because the gap edges in $N(E)$ are smeared in Fig. 5(b) by the screening current at high fields. Thus, subband-resolved DOS in Fig. 5(d) is not largely enhanced when it appears with increasing H in case (ii).

If observations about the H dependence of DOS in Fig. 5 are realized, such as by point-contact tunneling junction at the surface, we may examine the multigap structure of subbands in the superconductivity of the electric-field-induced surface metallic state from the detailed structure of the H dependence. The differences between cases (i) and (ii) may be used to estimate the ratio of the diamagnetic pair-breaking effect to the paramagnetic one from the experimental data. The ratio may be changed by the material parameter and experimental conditions. When effective mass m^* is larger as in the present calculations or when the superconducting region near the surface is thinner by tuning gate voltage, the diamagnetic pair-breaking effect is weakened, and the paramagnetic pair-breaking effect becomes dominant. In the opposite case of smaller m_0 or a thicker superconducting region, the diamagnetic pair-breaking effect becomes important, where the first-order transition at H_c may change to the second-order transition.

VI. PARAMAGNETIC SPIN DENSITY

The subband contributions are also seen in the paramagnetic spin density $m(z)$. Due to the Zeeman shift of the paramagnetic

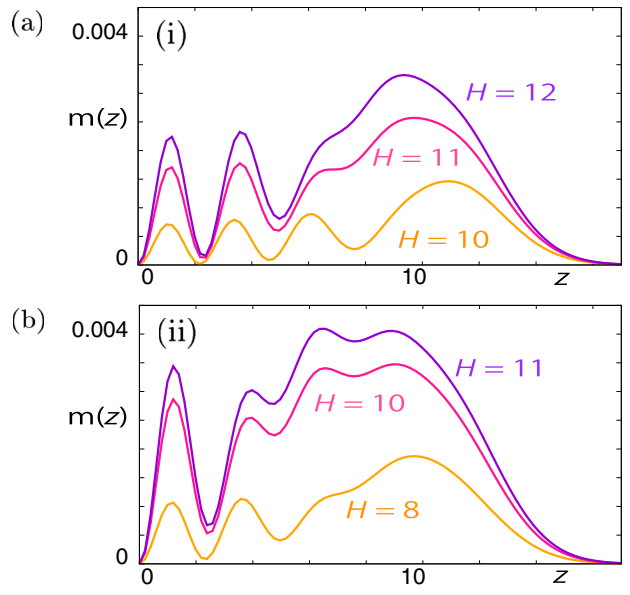

FIG. 6. (a) Depth z dependence of local spin density $m(z) = n_{\uparrow}(z) - n_{\downarrow}(z)$ at $H = 10$, 11, and 12 for case (i). (b) The same as (a), but for $H = 8$, 10, and 11 for case (ii).

effect, finite $m(z)$ appears, corresponding to the Knight shift. Figure 6(a) presents the spatial variation of $m(z)$ in case (i) for some fields H. Since the imbalance of up and down spins comes from the suppressed region of the subband-dependent superconductivity, $m(z)$ is larger in the deep region because of the higher-level subband contributions. The oscillating behavior of $m(z)$ at $H = 10$ reflects the oscillation of wave functions of higher-level subbands $i_z = 4$ and 5. With increasing H, contributions of lower-level subbands appear in addition to those of higher-level subbands, so that the oscillating behavior of $m(z)$ is smeared in the deep region. Figure 6(b) shows $m(z)$ in case (ii). We see oscillating behaviors similar to those in Fig. 6(a). In case (ii), $m(z)$ is larger from low fields since the pair potential $\langle\Delta\rangle$ is smaller because of the diamagnetic pair breaking in addition to the paramagnetic pair breaking.

Next, we present H dependences of the total paramagnetic moment $M_s = \int_0^\infty m(z)dz$ in Fig. 7(a) and the subband decompositions in Figs. 7(b) and 7(c). M_s is zero at low fields and appears from the middle fields. There, M_s is constructed of contributions from higher-level subbands. In case (i), the steplike increase in M_s occurs when contributions of lower-level subbands are added, as seen in Fig. 7(b). Also in case (ii), contributions of lower-level subbands are successively added with increasing H, as presented in Fig. 7(c). However, the steplike increase is smeared. This behavior comes from the smearing of the gap structure in Fig. 5(b) by the diamagnetic pair breaking due to the screening current.

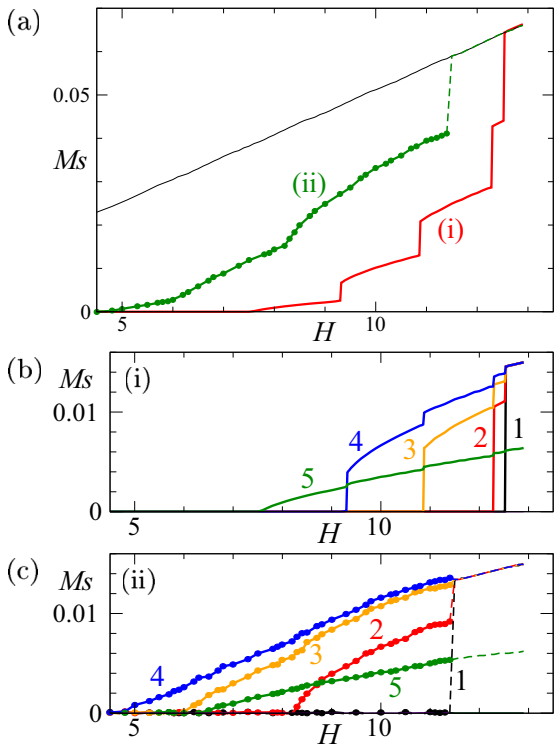

FIG. 7. (a) H dependence of total paramagnetic moment M_s in cases (i) and (ii). The straight line is for M_s in the normal state. (b) Subband decompositions ($i_z = 1, \ldots, 5$) of M_s in case (i) as a function of H. (c) The same as (b), but for case (ii).

VII. SUMMARY

The roles of paramagnetic and diamagnetic pair-breaking effects of parallel magnetic fields were evaluated in the superconductivity of the electric-field-induced surface metallic state based on calculations of the BdG equation. The depth dependences of the pair potential, current, spin current, internal field, and paramagnetic spin density were understood by using the subband contributions. With increasing magnetic fields H, the electronic states of the subbands become normal-state-like successively from higher-level subbands to lower-level ones, reflecting multigap superconductivity. This is reflected in the H dependence of the Fermi-energy DOS $N(E_F)$ and total paramagnetic moment M_s. We found that steps or peaks in the H dependence due to the paramagnetic pair breaking are smeared by the diamagnetic pair-breaking effect because the superconducting gap in higher-level subbands becomes gapless as a result of the contributions of the screening current. As only the paramagnetic pair-breaking effect was studied without including the diamagnetic effect in previous theoretical studies, the present study showed that the diamagnetic screening current induces another important pair-breaking effect even under parallel magnetic fields. We expect that observation of the H dependence, such as by a point-contact tunneling junction at the surface, may be a clue to examining the multigap structure and the pair-breaking effects of magnetic fields in the superconductivity of the electric-field-induced surface metallic state.

ACKNOWLEDGMENT

This work was supported by JSPS KAKENHI Grant No. 25400373.

APPENDIX: BdG EQUATION IN THE PRESENCE OF THE PARAMAGNETIC EFFECT

If we consider all possible spin pairings, the BCS Hamiltonian is given by a 4×4 matrix with a base $(\hat\psi_\uparrow,\hat\psi_\downarrow,\hat\psi_\uparrow^\dagger,\hat\psi_\downarrow^\dagger)$ of field operators for up- and down-spin electrons. However, here, we consider only the pairing between up- and down-spin electrons, neglecting spin-triplet equal spin pairing. Thus the BCS Hamiltonian is reduced to a 2×2 matrix as

$$\int d\mathbf{r}(\hat\psi_\uparrow^\dagger(\mathbf{r}) \quad \hat\psi_\downarrow(\mathbf{r}))\begin{pmatrix}K_\uparrow(\mathbf{r}) & \Delta(\mathbf{r})\\ \Delta^*(\mathbf{r}) & -K_\downarrow^*(\mathbf{r})\end{pmatrix}\begin{pmatrix}\hat\psi_\uparrow(\mathbf{r})\\ \hat\psi_\downarrow^\dagger(\mathbf{r})\end{pmatrix}, \tag{A1}$$

with $K_{\uparrow/\downarrow}(\mathbf{r})=(\hbar^2/2m^*)(-i\nabla+\frac{\pi}{\phi_0}\mathbf{A})^2\mp\mu_B H-\mu$. We note that $K_\uparrow(\mathbf{r})\neq K_\downarrow(\mathbf{r})$ in the presence of the paramagnetic effect because of the Zeeman energy. Following the method in Refs. [11,18,19,26,27], by a unitary transformation

$$\begin{pmatrix}\hat\psi_\uparrow(\mathbf{r})\\ \hat\psi_\downarrow^\dagger(\mathbf{r})\end{pmatrix}=\sum_\varepsilon\begin{pmatrix}u_{1\varepsilon}(\mathbf{r}) & -v_{2\varepsilon}^*(\mathbf{r})\\ v_{1\varepsilon}(\mathbf{r}) & u_{2\varepsilon}^*(\mathbf{r})\end{pmatrix}\begin{pmatrix}\hat\gamma_{1\varepsilon}\\ \hat\gamma_{2\varepsilon}^\dagger\end{pmatrix}, \tag{A2}$$

we diagonalize the Hamiltonian in Eq. (A1) as

$$\begin{pmatrix}u_{1\varepsilon'} & -v_{2\varepsilon'}^*\\ v_{1\varepsilon'} & u_{2\varepsilon'}^*\end{pmatrix}^{-1}\begin{pmatrix}K_\uparrow(\mathbf{r}) & \Delta(\mathbf{r})\\ \Delta^*(\mathbf{r}) & -K_\downarrow^*(\mathbf{r})\end{pmatrix}\begin{pmatrix}u_{1\varepsilon} & -v_{2\varepsilon}^*\\ v_{1\varepsilon} & u_{2\varepsilon}^*\end{pmatrix}$$
$$=\begin{pmatrix}E_{1\varepsilon} & 0\\ 0 & -E_{2\varepsilon}\end{pmatrix}\delta_{\varepsilon',\varepsilon}. \tag{A3}$$

The label of the eigenstate ε is given by $\varepsilon=(k_x,k_y,i_z)$ in this work. From Eq. (A3), the BdG equation is obtained as

$$\begin{pmatrix}K_\uparrow(\mathbf{r}) & \Delta(\mathbf{r})\\ \Delta^*(\mathbf{r}) & -K_\downarrow^*(\mathbf{r})\end{pmatrix}\begin{pmatrix}u_\epsilon(\mathbf{r})\\ v_\epsilon(\mathbf{r})\end{pmatrix}=E_\epsilon\begin{pmatrix}u_\epsilon(\mathbf{r})\\ v_\epsilon(\mathbf{r})\end{pmatrix}, \tag{A4}$$

where

$$\begin{pmatrix}u_\epsilon(\mathbf{r})\\ v_\epsilon(\mathbf{r})\end{pmatrix}=\begin{pmatrix}u_{1\varepsilon}(\mathbf{r})\\ v_{1\varepsilon}(\mathbf{r})\end{pmatrix},\begin{pmatrix}-v_{2\varepsilon}^*(\mathbf{r})\\ u_{2\varepsilon}^*(\mathbf{r})\end{pmatrix} \tag{A5}$$

for $E_\epsilon=E_{1\varepsilon}$ and $-E_{2\varepsilon}$, respectively. In the case of $K_\uparrow(\mathbf{r})=K_\downarrow(\mathbf{r})$, we have the relations $E_{1\varepsilon}=E_{2\varepsilon}$, $u_{1\varepsilon}(\mathbf{r})=u_{2\varepsilon}(\mathbf{r})$, and $v_{1\varepsilon}(\mathbf{r})=v_{2\varepsilon}(\mathbf{r})$. In many cases solving the BdG equation, eigenstates are divided into two groups: positive eigenenergies $E_{1\varepsilon}$ with $(u_{1\varepsilon}(\mathbf{r}),v_{1\varepsilon}(\mathbf{r}))$ and negative ones $-E_{2\varepsilon}$ with $(-v_{2\varepsilon}^*(\mathbf{r}),u_{2\varepsilon}^*(\mathbf{r}))$. However, here, we combine two groups of the eigenstates using the unified notation E_ϵ, $u_\epsilon(\mathbf{r})$, $v_\epsilon(\mathbf{r})$ in Eq. (A5). There, eigenstates are labeled by $\epsilon=(\varepsilon,\alpha)$ with α for two states of $E_{1\varepsilon}$ and $-E_{2\varepsilon}$.

By the unitary transformation, densities of up- and down-spin electrons are calculated as

$$n_\uparrow(\mathbf{r})=\langle\hat\psi_\uparrow^\dagger(\mathbf{r})\hat\psi_\uparrow(\mathbf{r})\rangle$$
$$=\sum_\varepsilon\{|u_{1\varepsilon}(\mathbf{r})|^2f(E_{1\varepsilon})+|v_{2\varepsilon}^*(\mathbf{r})|^2f(-E_{2\varepsilon})\}, \tag{A6}$$

$$n_\downarrow(\mathbf{r})=\langle\hat\psi_\downarrow^\dagger(\mathbf{r})\hat\psi_\downarrow(\mathbf{r})\rangle$$
$$=\sum_\varepsilon\{|v_{1\varepsilon}(\mathbf{r})|^2f(-E_{1\varepsilon})+|u_{2\varepsilon}^*(\mathbf{r})|^2f(E_{2\varepsilon})\}, \tag{A7}$$

where $\langle\cdots\rangle$ indicates the statistical average. Similarly, the y component of up- and down-spin currents is given by

$$J_\uparrow(\mathbf{r})=\mathrm{Re}\langle\hat\psi_\uparrow^\dagger(\mathbf{r})\hat F\hat\psi_\uparrow(\mathbf{r})\rangle$$
$$=\sum_\varepsilon\mathrm{Re}\{u_{1\varepsilon}^*(\mathbf{r})\hat F u_{1\varepsilon}(\mathbf{r})f(E_{1\varepsilon})$$
$$-v_{2\varepsilon}(\mathbf{r})\hat F v_{2\varepsilon}^*(\mathbf{r})f(-E_{2\varepsilon})\}, \tag{A8}$$

$$J_\downarrow(\mathbf{r})=\mathrm{Re}\langle\hat\psi_\downarrow^\dagger(\mathbf{r})\hat F\hat\psi_\downarrow(\mathbf{r})\rangle$$
$$=\sum_\varepsilon\mathrm{Re}\{v_{1\varepsilon}(\mathbf{r})\hat F v_{1\varepsilon}^*(\mathbf{r})f(-E_{1\varepsilon})$$
$$+u_{2\varepsilon}^*(\mathbf{r})\hat F u_{2\varepsilon}(\mathbf{r})f(E_{2\varepsilon})\}, \tag{A9}$$

with $\hat F=(e\hbar/m^*)(-i\partial_y+\frac{\pi}{\phi_0}A_y)$. The pair potential is given by the gap equation

$$\Delta(\mathbf{r})\equiv V_{\mathrm{pair}}\langle\hat\psi_\uparrow(\mathbf{r})\hat\psi_\downarrow(\mathbf{r})\rangle$$
$$=V_{\mathrm{pair}}{\sum_\varepsilon}'\{u_{1\varepsilon}(\mathbf{r})v_{1\varepsilon}^*(\mathbf{r})f(-E_{1\varepsilon})-v_{2\varepsilon}^*(\mathbf{r})u_{2\varepsilon}(\mathbf{r})f(E_{2\varepsilon})\}. \tag{A10}$$

Using the notation in Eq. (A5), Eqs. (A6)–(A10) are written as

$$n_\uparrow(\mathbf{r})=\sum_\epsilon|u_\epsilon(\mathbf{r})|^2f(E_\epsilon), \tag{A11}$$

$$n_\downarrow(\mathbf{r})=\sum_\epsilon|v_\epsilon(\mathbf{r})|^2f(-E_\epsilon), \tag{A12}$$

$$\Delta(\mathbf{r})=V_{\mathrm{pair}}{\sum_\epsilon}'u_\epsilon(\mathbf{r})v_\epsilon^*(\mathbf{r})f(-E_\epsilon), \tag{A13}$$

$$J_\uparrow(\mathbf{r})=\sum_\epsilon\mathrm{Re}\{u_\epsilon^*(\mathbf{r})\hat F u_\epsilon(\mathbf{r})f(E_\epsilon)\}, \tag{A14}$$

$$J_\downarrow(\mathbf{r})=\sum_\epsilon\mathrm{Re}\{v_\epsilon(\mathbf{r})\hat F v_\epsilon^*(\mathbf{r})f(-E_\epsilon)\}. \tag{A15}$$

Substituting Eq. (1) into these equations, we obtain Eqs. (4)–(8). This formulation of the BdG equation with $K_\uparrow(\mathbf{r})\neq K_\downarrow(\mathbf{r})$ was used in previous studies for an inhomogeneous superconducting state coexisting with the spin-density wave [26,27] and the superfluid phase of a trapped Fermion gas with a population imbalance of up and down spins [18,19].

[1] K. Ueno, H. Shimotani, H. Yuan, J. T. Ye, M. Kawasaki, and Y. Iwasa, J. Phys. Soc. Jpn. **83**, 032001 (2014).

[2] K. Ueno, S. Nakamura, H. Shimotani, A. Ohtomo, N. Kimura, T. Nojima, H. Aoki, Y. Iwasa, and M. Kawasaki, Nat. Mater. **7**, 855 (2008).

[3] J. T. Ye, S. Inoue, K. Kobayashi, Y. Kasahara, H. T. Yuan, H. Shimotani, and Y. Iwasa, Nat. Mater. **9**, 125 (2010).

[4] K. Ueno, S. Nakamura, H. Shimotani, H. T. Yuan, N. Kimura, T. Nojima, H. Aoki, Y. Iwasa, and M. Kawasaki, Nat. Nanotechnol. **6**, 408 (2011).

[5] K. Taniguchi, A. Matsumoto, H. Shimotani, and H. Takagi, Appl. Phys. Lett. **101**, 042603 (2012).

[6] J. T. Ye, Y. J. Zhang, R. Akashi, M. S. Bahramy, R. Arita, and Y. Iwasa, Science **338**, 1193 (2012).

[7] J. Biscaras, N. Bergeal, S. Hurand, C. Grossetête, A. Rastogi, R. C. Budhani, D. LeBoeuf, C. Proust, and J. Lesueur, Phys. Rev. Lett. **108**, 247004 (2012).

[8] J. A. Bert, K. C. Nowack, B. Kalisky, H. Noad, J. R. Kirtley, C. Bell, H. K. Sato, M. Hosoda, Y. Hikita, H. Y. Hwang, and K. A. Moler, Phys. Rev. B **86**, 060503 (2012).

[9] A. F. Santander-Syro, O. Copie, T. Kondo, F. Fortuna, S. Pailhès, R. Weht, X. G. Qiu, F. Bertran, A. Nicolaou, A. Taleb-Ibrahimi, P. Le Fèvre, G. Herranz, M. Bibes, N. Reyren, Y. Apertet, P. Lecoeur, A. Barthélémy, and M. J. Rozenberg, Nature (London) **469**, 189 (2011).

[10] P. D. C. King, S. M. Walker, A. Tamai, A. de la Torre, T. Eknapakul, P. Buaphet, S.-K. Mo, W. Meevasana, M. S. Bahramy, and F. Baumberger, Nat. Commun. **5**, 3414 (2014).

[11] Y. Mizohata, M. Ichioka, and K. Machida, Phys. Rev. B **87**, 014505 (2013).

[12] A. A. Shanenko, M. D. Croitoru, R. G. Mints, and F. M. Peeters, Phys. Rev. Lett. **99**, 067007 (2007); A. A. Shanenko, M. D. Croitoru, and F. M. Peeters, Phys. Rev. B **78**, 054505 (2008); Y. Chen, A. A. Shanenko, and F. M. Peeters, *ibid.* **81**, 134523 (2010).

[13] A. A. Shanenko, M. D. Croitoru, A. Vagov, and F. M. Peeters, Phys. Rev. B **82**, 104524 (2010); A. A. Shanenko, M. D. Croitoru, A. V. Vagov, V. M. Axt, A. Perali, and F. M. Peeters, Phys. Rev. A **86**, 033612 (2012).

[14] A. A. Shanenko, M. D. Croitoru, and F. M. Peeters, Phys. Rev. B **78**, 024505 (2008).

[15] M. D. Croitoru, A. A. Shanenko, C. C. Kaun, and F. M. Peeters, Phys. Rev. B **80**, 024513 (2009).

[16] Y. Chen, A. A. Shanenko, M. D. Croitoru, and F. M. Peeters, J. Phys. Condens. Matter **24**, 265702 (2012).

[17] P. G. de Gennes, *Superconductivity of Metals and Alloys* (Addison-Wesley, Reading, MA, 1989).

[18] T. Mizushima, K. Machida, and M. Ichioka, Phys. Rev. Lett. **94**, 060404 (2005).

[19] M. Takahashi, T. Mizushima, M. Ichioka, and K. Machida, Phys. Rev. Lett. **97**, 180407 (2006).

[20] M. W. Zwierlein, A. Schirotzek, C. H. Schunck, and W. Ketterle, Science **311**, 492 (2006).

[21] M. W. Zwierlein, C. H. Schunck, A. Schirotzek, and W. Ketterle, Nature (London) **442**, 54 (2006).

[22] K. Ueno, T. Nojima, S. Yonezawa, M. Kawasaki, Y. Iwasa, and Y. Maeno, Phys. Rev. B **89**, 020508 (2014).

[23] M. Nabeta, K. K. Tanaka, S. Onari, and M. Ichioka, Physica C (Amsterdam, Neth.) **530**, 8 (2016).

[24] P. Fulde and R. A. Ferrell, Phys. Rev. **135**, A550 (1964).

[25] A. I. Larkin and Y. N. Ovchinnikov, Sov. Phys. JETP **20**, 762 (1965).

[26] M. Ichioka, M. Takigawa, and K. Machida, J. Phys. Soc. Jpn. **70**, 33 (2001).

[27] M. Takigawa, M. Ichioka, and K. Machida, Phys. Rev. Lett. **90**, 047001 (2003).